The Role of the S_1 State of Carotenoids in Photosynthetic Energy Transfer: The Light-Harvesting Complex II of Purple Bacteria

Chao-Ping Hsu,[†] Peter J. Walla,[†] Martin Head-Gordon,[†,‡] and Graham R. Fleming*[,†,§]

Department of Chemistry, University of California, Berkeley, California 94720-1460, and Chemical Sciences Division and Physical Biosciences Division, Lawrence Berkeley National Laboratory, Berkeley, California 94720

Received: May 22, 2001

Using time-dependent density functional theory (TDDFT), we obtained the excitation energy transfer coupling (Coulombic coupling) between the S_1 state of rhodopin glucoside (RG) and the Q_y state of bacteriochlorophylls (BChl) in the light-harvesting complex II (LH2) of purple photosynthetic bacterium *Rhodopseudomonas (Rps.) acidophila*. Our results suggest that the small mixing of S_2 character arising from symmetry-breaking of the carotenoid plays an important role in the Coulombic coupling. As a result the carotenoid (car) S_1 couplings to chlorophylls are similar to a set of scaled down Car(S_2)−BChl(Q_y) couplings. We also report results for 6,10,15,19-tetramethyl-2-*cis*-4,6,8,10,12,14,16,18,20-*all trans*-22-*cis*-tetracosaundecaene, the polyene backbone of RG with six methyl groups attached, in two different structures: an optimized planar structure and the crystal structure of RG with hydrogen atoms replacing the two end groups, which is distorted from its planar structure. The mixing of S_2 configuration is strictly forbidden in the planar structure due to symmetry. In this case the polyene still couples moderately strongly to the nearby BChls. In the distorted structure derived from RG crystal structure, coupling strengths and the role of S_2 character mixing are similar to those of the full RG. Using an exciton model simulation, the calculated coupling strengths yield Car(S_1)-to-BChl(Q_y) excitation energy transfer times that are in good agreement with recent experimental results.

I. Introduction

Ultrafast spectroscopy allows the excitation energy transfer (EET) among photosynthetic antenna pigments to be monitored in detail.[1] The role of carotenoids (Car) in photosynthesis has been the focus of much recent study. It has long been observed that some carotenoids are able to transfer their excitation energy to chlorophylls (Chl) to drive photochemistry.[2−4] It is now generally accepted that carotenoids extend the spectral coverage of the antenna system and help collect solar energy with chlorophylls or bacteriochlorophylls (BChl).[5,6] In addition to this light-harvesting function, carotenoids are also involved in photoprotection via triplet quenching and direct reaction with singlet oxygen (see, for example, ref 7 and references therein). This article will focus solely on the light-harvesting function of carotenoids and the mechanism of their interaction with the BChl molecules of a light-harvesting antenna system, light-harvesting complex II (LH2) of purple bacteria. This system provides an ideal test bed for such studies since the crystal structure of the complex has been determined to high resolution for two species,[8,9] and over the past several years many research groups have attempted to address how energy transfer may occur in the LH2 complex of purple bacteria, both experimentally and theoretically.[10−22]

Carotenoids are generally described by analogy to polyenes: their ground state (S_0) and first excited state (S_1) are both of A_g symmetry. Thus the $S_0 \rightarrow S_1$ transition is one-photon forbidden. The second excited state (S_2) is of B_u symmetry and carries a large oscillator strength. It has been experimentally demonstrated that carotenoids can transfer their excitation energy from the S_2 state, by an efficient EET coupling, to the Q_x and Q_y states of BChls.[10−12] Competing with this process is ultrafast internal conversion from S_2 to S_1. It is then of interest to determine whether the carotenoid S_1 state can effectively transfer its excitation energy to its neighboring BChls. Important early observations of the role of the S_1 state were made by Shreve et al.[14] via excitation of the strongly allowed S_0-S_2 transition. Definitive evidence of S_1 to BChl energy transfer was provided by Krueger et al.[15] In this work the S_1 state was directly excited by two photon absorption and the energy transfer monitored by detecting fluorescence from the BChl molecules. In subsequent work the S_1 lifetimes were measured in LH2 complexes from two species of purple bacteria: *Rhodobacter (Rb.) sphaeroides* and *Rhodopseudomonas (Rps.) acidophila*.[16]

The forbidden transition from the ground state to the S_1 state of carotenoids has a very small transition dipole moment. The Förster dipole coupling scheme[23] cannot be used to estimate the coupling strength. Quadrupole−dipole coupling and the Dexter exchange coupling[24] have been suggested as candidates for possible coupling mechanisms.[17] In ref 18, the weak emission from the S_1 state, possibly arising from vibronic coupling, was monitored for carotenoids *in solution*. The transition dipole moments of the $S_0 \rightarrow S_1$ transition were estimated to be 4−6% of those of the $S_0 \rightarrow S_2$ transition. Assuming the Coulombic coupling is proportional to the magnitude of transition dipole moment and assuming that the spectral properties of carotenoids in solution are similar to those in LH2 complexes, the authors use this 4−6% factor to scale down a set of Car(S_2)−BChl(Q_y) couplings, obtained from a semiempirical calculation,[20] for an

[†] University of California.
[‡] Chemical Sciences Division, Lawrence Berkeley National Laboratory.
[§] Physical Biosciences Division, Lawrence Berkeley National Laboratory.

10.1021/jp0119835 CCC: $20.00
Published on Web 10/17/2001

estimate of Car(S_1)−BChl(Q_y) Coulombic coupling. The result is encouraging, but it does not reproduce the large differences in EET rate among LH2 complexes from different species.

Before X-ray crystallographic data for LH2 were available, Nagae et al.[17] reported calculated rates for Car → BChl excitation energy transfer and gave the relative magnitudes of Coulombic coupling and the Dexter exchange coupling from a semiempirical calculation, using a perfect, nondistorted geometry of the conjugated portion of BChl *a* and neurosporene. The authors found that the exchange couplings are much smaller than the corresponding Coulombic coupling strengths. Moreover, the coupling to BChl from the S_1 ($2\ ^1A_g$) state of the carotenoid was found to be 2 orders of magnitude smaller than that from the S_2 ($1\ ^1B_u$) state. Shortly after the crystal structure of LH2 became available, Alden et al. performed a semiempirical molecular orbital calculation for couplings between the two groups of BChl aggregates (B800 and B850) in the LH2 complex of *Rps. acidophila*, in which a simple distance-dependent dielectric screening was assumed.[19] The main features of the absorption and CD spectra for the BChls are reproduced and a comprehensive description of the delocalization of excitation over the B850 and B800 aggregates were reported, but the role of the carotenoid in EET was not addressed. Damjanović et al. calculated the EET coupling between Car and BChl for *Rhodospirillum (Rs.) molischianum*, using a semiempirical Hamiltonian in a configuration-interaction (CI) calculation.[20] The authors reported a calculated EET rate from the S_2 state of carotenoids that is close to the experimental value, while for the S_1 state, the calculated rate was 2 orders of magnitude smaller than the observed value. The first ab initio level of quantum calculations for the couplings in LH2 are perhaps those performed by Krueger et al.[21] and Scholes et al.[22] A simple excited-state method, configuration interaction with single excitation (CIS), was used. The Coulombic coupling, the most important contribution to the EET coupling, was computed from the transition density cube (TDC), a full-space numerical Rieman-summation method. This work reported the calculated coupling between the allowed S_2 state and BChls. The S_1 state of carotenoids has significant double excitation character, and the CIS method does not offer a satisfactory description for such a state.

Time-dependent density functional theory (TDDFT) has been developed and formulated for a variety of purposes.[25−28] For calculating excitation energies,[29−33] the computational cost and complexity of TDDFT is roughly comparable to single excitation theories based on a Hartree−Fock ground state, such as single excitation CI (CIS) or the random phase approximation (RPA). At the same time, excitation energies to valence excited states are considerably improved,[30−33] and there is even significant improvement for excitation energies of excited states that, when treated by wave function-based methods, have appreciable double excitation character.[34,35] These attractive characteristics have enabled TDDFT to be applied to a number of large systems (for example, see refs 36 and 37). The Tamm−Dancoff approximation to TDDFT (TDDFT/TDA)[38] is also employed in the present study. The TDA was proposed as a simple approximation to TDDFT by realizing that, within TDDFT, most of the excitation processes were simple transitions of an electron from an occupied orbital to an unoccupied orbital. This is generally true, as has already been demonstrated.[38] Recently, TDDFT and TDDFT/TDA have been tested for linear polyene oligomers,[39] which are thought to have excited-state character similar to carotenoids. It was found that both TDDFT and TDDFT/TDA are capable of describing the $2\ ^1A_g$ state, giving similar results for excitation energies close to the experimental values. However, for the $2\ ^1B_u$ state, the excitation energy is underestimated by 0.5 eV with TDDFT, while TDDFT/TDA consistently gives an excitation energy closer to the experimental value. For a self-consistent calculation of the energy transfer couplings, it is also necessary to calculate the electronic structure of the acceptor (BChl) molecules via TDDFT. TDDFT has recently been applied to calculate the excitation spectrum for chlorophyll *a*.[36,37] The author reported negligible effects of the phytyl group on the lowest six excited states. Four states in the region of the Q-bands, seven transitions in the B (Soret) band region, and two weak transitions between the two bands were also reported. The additional electronic states may be a result of underestimating the energies of the Rydberg states higher in excitation energy, since this is a known problem in TDDFT.[40] However, it is perhaps the first ab initio calculation of chlorophyll that does not involve a selection of active electron and active space. It is possible, though not very likely, that traditional theories restricted to excitation among the π electrons and π orbitals are not sufficient to fully describe all the electronic states in the visible frequency region. More work is needed to confirm the existence of those additional electronic states.

In this paper we report the results of our TDDFT calculations of the EET coupling between the Car(S_1) and BChl(Q_y) states using the crystal structure of light-harvesting complex II (LH2) of *Rps. acidophila* strain 10500.[8] The overall Car(S_1) to BChl(Q_y) EET rate is also calculated for a comparison with recent experimental results.

II. Theory and Calculation

A detailed derivation of EET coupling based on TDDFT was given in ref 41. The result parallels (and is similar to) the conventional configuration-interaction (CI) based expression. The energy transfer coupling for a pair of donor (D) and acceptor (A) molecules is

$$U_{DA}^0 = \int d\mathbf{r} \int d\mathbf{r}'\, \rho_D^{T*}(\mathbf{r})\left(\frac{1}{|\mathbf{r}-\mathbf{r}'|} + g_{XC}(\mathbf{r},\mathbf{r}',\omega_0)\right)\rho_A^T(\mathbf{r}') - \omega_0 \int d\mathbf{r}\, \rho_D^{T*}(\mathbf{r})\, \rho_A^T(\mathbf{r}) \quad (1)$$

where $\rho^T(\mathbf{r})$ is the transition density of the donor or acceptor molecule, defined as diagonal elements of the transition density matrix $\tilde{\rho}^T(\mathbf{r},\mathbf{r}')$

$$\rho^T(\mathbf{r}) = \tilde{\rho}^T(\mathbf{r},\mathbf{r}) \quad (2)$$

$$\tilde{\rho}^T(\mathbf{r},\mathbf{r}') = N \int ... \int d\mathbf{r}_2\, d\mathbf{r}_3 ... d\mathbf{r}_N\, \psi_{ex}(\mathbf{r},\mathbf{r}_2,\mathbf{r}_3,...,\mathbf{r}_N)\, \psi_{gr}^*(\mathbf{r}',\mathbf{r}_2,\mathbf{r}_3,...,\mathbf{r}_N) \quad (3)$$

and $g_{XC}(\mathbf{r},\mathbf{r}',\omega)$ is the Fourier transform of $g_{XC}(\mathbf{r},t;\mathbf{r}',t')$, which is the exchange-correlation kernel:

$$g_{XC}(\mathbf{r},t;\mathbf{r}',t') = \frac{\delta^2 A_{XC}[\rho]}{\delta\rho(\mathbf{r},t)\, \delta\rho(\mathbf{r}',t')} \quad (4)$$

$A_{XC}[\rho(\mathbf{r},t)]$ is the exchange-correlation functional.[27,29]

The first term on the RHS of eq 1 consists of two contributions: The integration with $1/|\mathbf{r}-\mathbf{r}'|$ is the *Coulomb* interaction, while the term with g_{XC} arises from the *exchange-correlation* effect between the transition density of the donor (D) and acceptor (A). The second term at the RHS of eq 1 is an overlap effect, which is normally expected to be a small effect and is

SCHEME 1: Chemical Structures for Carotenoid Rhodopin Glucoside (RG) and Its Analog, 6,10,15,19-Tetramethyl-2-*cis*-4,6,8,10,12,14,16,18,20-*all trans*-22-*cis*-tetracosaundecaene (I)

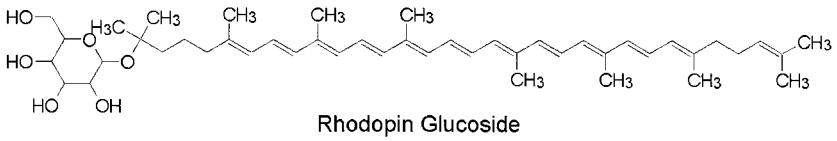

Rhodopin Glucoside

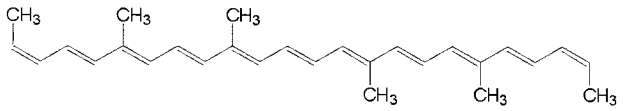

I

often ignored. Exchange effects have been shown to be much smaller in refs 17 and 20, and we therefore focus our attention on the Coulombic coupling, which is calculated with the transition density cube (TDC) technique.[21]

The formalism and applications of TDDFT have been reported previously (see ref 35, for example) and are not repeated here. The transition densities are generated with a development version of Q-Chem[42] for each pigment, rhodopin glucoside (RG) and bacteriochlorophyll *a* (BChl). The structures of RG and BChl are obtained as in our earlier work:[21] positions for heavy atoms are taken from the crystal structure,[8] while hydrogen atoms are added and optimized in the ground state with a MNDO calculation. There is only a small change in our results (less than 0.05 eV in excitation energy) when the position of hydrogen atoms are optimized in a hybrid Becke3-Lee−Yang−Parr (B3LYP) functional[43] with the 6-31G** basis set. According to our previous studies of polyene oligomers,[39] we choose to use the SVWN functional[44,45] with the 6-31++G** basis set for all of our excited-state calculations. For the BChl calculations, the phytyl group is replaced by a hydrogen atom. Such a replacement caused negligible change in the excitation energies and oscillator strengths for the first six excited states of chlorophyll *a*.[36,37] We expect that this replacement would also have a negligible effect for BChl.

To investigate the role of symmetry-breaking produced by the distorted structure of the carotenoid in the protein matrix, we have also calculated the transition density for the S_0 to S_1 transition of 6,10,15,19-tetramethyl-2-*cis*-4,6,8,10,12,14,16,18,20-*all trans*-22-*cis*-tetracosaundecaene (**I**). This molecule has the polyene backbone of RG with 11 conjugated C−C double bonds and six methyl groups attached (Scheme 1). We have investigated two different geometries of the model molecule **I**. One is obtained directly from the crystal structure,[8] with hydrogen atoms replacing the two end groups. As stated above, this structure is distorted from its ground-state minimum-energy structure and has an out-of-plane bend. It will be referred to as the "distorted" structure below. The other structure of molecule **I** studied in the present work is a fully optimized planar ground-state structure obtained from a density functional calculation with 6-31G**/B3LYP.[43] In Figure 1 the optimized structure of molecule **I** is shown. The C_{2h} symmetry is retained; therefore there is no mixing of B_u character in the S_1 ($2\ ^1A_g$) state. This symmetric structure will be referred to as the "planar" structure below.

We have performed the calculation without considering the effect of the surrounding medium. In Figure 2 we plotted the transition density of S_1 transition, calculated with TDDFT/TDA with SVWN functional. It is seen to have alternating positive and negative charges aligned along the polyene chain. Such character may have induced a much smaller optical dielectric response in the surrounding medium compared to that from a simple transition dipole. In the future the effects of the medium should be studied. Instead of employing a simple scaling factor as done in the past,[19,46] we propose to use a more complete description derived recently,[41] which depends on the nature of the transition and the shape of the molecule.

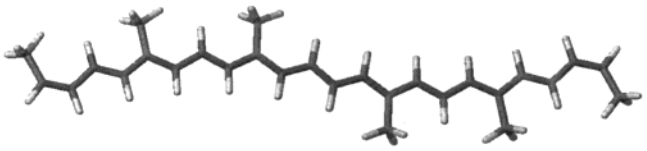

Figure 1. Optimized (planar) geometry of molecule **I**.

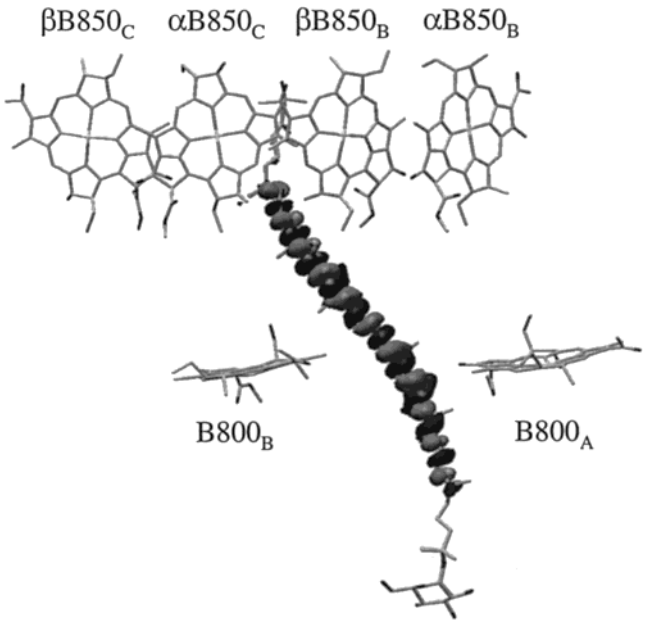

Figure 2. Transition density of $S_0 \rightarrow S_1$ of RG, calculated from TDDFT/TDA with SVWN functional. Light and dark shaded surfaces are contour surfaces for transition density with opposite phases (signs).

To calculate the coupling between the Q_y transition of BChls and the planar polyene molecule **I**, we need to replace the carotenoid, RG, in the crystal structure with the model molecules. For the distorted structure of molecule **I** this is trivial since the positions of the heavy atoms are from the crystal structure and there is no ambiguity in placing the model molecule into the crystal structure. For the planar structure there are a number of different choices for this transformation. In the present work we performed the transformation as stated below.

In making translations and rotations of an object in three-dimensional space, one needs to define the position of an origin for translation and two linearly independent axes for rotation. The translations and rotations are performed to bring the origin

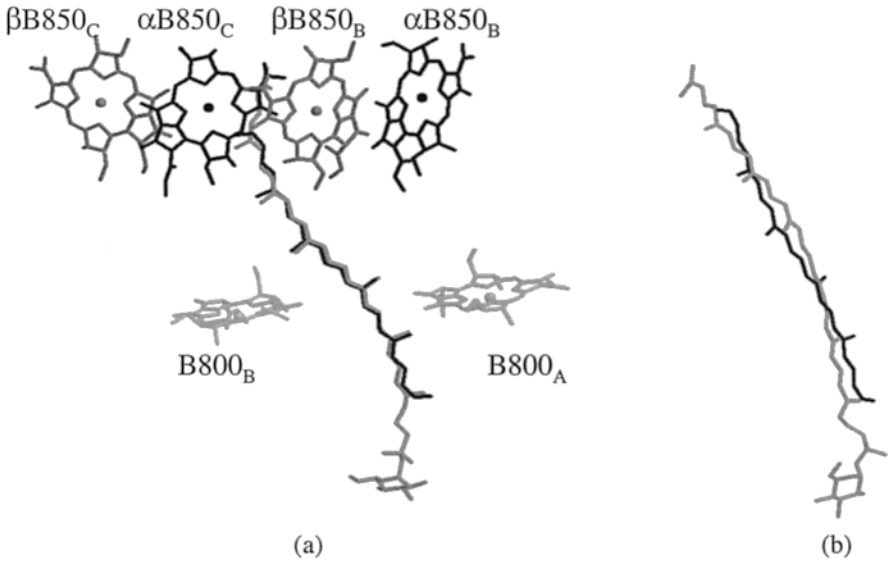

Figure 3. (a) Position of planar molecule **I** placed in the LH2 crystal structure in order to best represent a situation where the mixing of the 1 ^1B_u-like configuration does not occur. In (b) the same structure as in part (a) is plotted from a different viewing angle to show the difference in the geometry of planar molecules **I** and RG. The BChls are excluded in this plot for clarity.

and the two axes of the model molecule to coincide with those of the RG in the crystal structure. We have chosen the center-of-mass of carbon atoms of the conjugated backbone plus the six methyl carbons attached to the conjugated chain as the origin. The first axis is defined along the conjugated carbons by averaging the vectors going from any carbon atom to the next nearest one in the conjugated part of the molecule. The second axis used in defining the rotation is the averaged vector from the carbon atom with a methyl group attached in the conjugated chain to the methyl carbon. In this case there is some mismatch between a model molecule with C_{2h} symmetry and the distorted carotenoid in the crystal structure. We choose to match the origin by a translation, and the direction of the first axis is superimposed by a rotation. In 3-dimensional space, one can find a plane containing the origin and the two linearly independent vectors starting from the origin. Such planes from the model molecule and the crystal structure are superimposed by a second rotation. The final placement of the polyene in the LH2 complex is plotted in Figure 3.

In an LH2 complex, two-thirds of the BChls form a tightly coupled molecular aggregate, called B850, while the other one-third of the BChls form a less strongly coupled ring aggregate named B800. In such aggregates the transition dipole moments cancel for most of the excitonic states, leaving the optical spectra shifted, narrowed and deviating from the underlying density of states distribution. In this case Förster theory, which uses the optical spectra to account for the energy conservation factor, is not valid. To calculate the EET rate we have employed a model simulation to properly account for the coupling with the excitonic states of BChls in B850. In this simulation, we have calculated the density of the excitonic states formed by the BChls in B850. The coupling between BChls in B850 and the spectral line shape (homogeneous broadening, intramolecular vibrational frequencies, and displacements) of each excitonic state are all from ref 47. We have also included the effect of disorder by performing an ensemble average. Following previous work,[47] which gives a good account of EET between B800 and B850, we have included a Gaussian distribution for each BChl site energy. We have used the values of 0.020 eV for BChls in B850 and 0.009 eV for BChls in B800 for the standard deviation in the distribution of site energy. The ensemble average is performed *after* taking the product of coupling strength and the spectral overlap, which is the "EET rate" for each ensemble, as outlined in ref 16 and described previously in ref 47. In this work all the EET time constants reported are within 4% statistical error due to random sampling.

TABLE 1: First Four Singlet Excited States of Rhodopin Glucoside (RG), Obtained from TDDFT/TDA and TDDFT Calculations Using the SVWN Functionals and 6-31++G Basis Set**

state	E^a	λ^b	f^c	μ^d	λ(exp)^b	μ(exp)^d
			TDDFT/TDA			
S_1	1.47	844.3	0.02	1.73		
S_2	1.94	639.7	1.84	15.8	418, 401[e]	13[e]
	2.10	589.5	1.15	12.0		
	2.15	576.1	5.90	26.9		
			TDDFT			
S_1	1.46	848.6	0.25	6.66		
S_2	1.57	788.7	3.16	23.0		
	1.98	627.3	0.06	2.83		
	2.11	588.7	0.01	1.02		

[a] Excitation energies in electronvolts. [b] Excitation wavelengths in nanometers. [c] Oscillator strengths. [d] Transition dipole moments in Debye. [e] Reference 58. The excitation wavelengths are absorption maxima for carotenoids with the same number (11) of conjugated double bonds as RG, namely, lycopene and β-carotene, respectively. Listed values are extrapolated to the gas-phase values.

In determining the EET rate from the calculated coupling strengths, we need the position and spectral density of the Car S_1 state. We assumed that the S_1 states of the carotenoids have the same emission spectral line shape as that of spheroidene, which was obtained from the mirror image of the two-photon excitation spectrum.[15]

III. Results

The results of our TDDFT and TDDFT/TDA calculations for RG are summarized in Table 1. When compared with experimental results of similar carotenoids, the calculated excitation energy for the S_2 state is lower by almost 1 eV (TDDFT/TDA). In a recent work,[48] the excitation energies are calculated, with the state-averaged complete active space SCF method, for a carotenoid molecule in a charge field created by its surrounding proteins and BChls. These results are close to the experimentally observed values for the S_2 state.

TABLE 2: Excited States of BChls from TDDFT/TDA and TDDFT Calculations with SVWN/6-31++G**

state	E^a	λ(calc)^b	f^c	μ^d	m^e m_x	m_y	m_z	λ(exp)^b	μ(exp)^d
B800									
TDDFT/TDA									
	1.83	676.1	0.00	0.30	−0.09	0.08	−0.01		
	1.93	642.9	0.04	2.30	0.37	−0.83	0.01		
Q_y	2.04	606.9	0.50	8.01	0.22	3.15	−0.04	773,[f] 772[g]	6.13[h]
Q_x	2.16	573.4	0.03	1.76	−0.69	0.06	−0.05	577,[f] 605−608[g]	3.29[h]
TDDFT									
Q_y	1.73	718.4	0.30	6.73	0.04	2.65	−0.04		
	1.83	676.3	0.00	0.74	−0.12	−0.27	0.00		
	1.92	644.5	0.03	1.93	0.52	0.55	0.00		
Q_x	2.10	589.2	0.02	1.71	−0.67	−0.06	−0.05		

state	E^a	λ^b	f^c	μ^d	m^e m_x	m_y	m_z
B850α							
TDDFT/TDA							
	1.70	729.7	0.01	0.91	−0.35	−0.08	0.00
Q_y	2.06	601.9	0.55	8.38	−0.27	−3.29	0.04
Q_x	2.14	580.5	0.03	2.02	−0.76	0.22	−0.01
	2.24	552.6	0.01	1.25	0.48	−0.09	−0.01
TDDFT							
	1.69	735.6	0.01	1.00	−0.39	0.06	−0.01
Q_y	1.76	703.8	0.34	7.10	−0.21	−2.79	0.04
Q_x	2.05	604.4	0.04	2.34	−0.92	−0.04	−0.01
	2.22	559.2	0.00	0.59	0.23	−0.03	−0.01
B850β							
TDDFT/TDA							
	1.68	737.3	0.00	0.34	−0.13	−0.03	0.00
Q_y	2.06	602.6	0.55	8.40	0.20	3.30	−0.11
Q_x	2.11	586.4	0.03	1.91	−0.74	0.11	0.00
	2.21	560.6	0.03	1.71	0.67	0.01	−0.02
TDDFT							
	1.68	738.6	0.00	0.36	−0.14	−0.02	0.00
Q_y	1.74	712.8	0.32	6.94	0.14	2.73	−0.10
Q_x	2.03	609.6	0.05	2.48	−0.97	−0.11	0.01
	2.18	569.9	0.00	0.76	0.30	0.00	−0.02

[a] Excitation energies in electronvolts. [b] Excitation wavelengths in nanometers. [c] Oscillator strengths. [d] Transition dipole moments in Debye. [e] Projection of transition dipole moments in atomic units. The Cartesian coordinate is defined with the *x*-axis along the N_A-Mg-N_C direction (averaged) and the *y*-axis pependicular to the *x*-axis, roughly along the N_D-Mg-N_B direction. N_A, N_B, N_C, and N_D are defined in the crystal structure data.[8] [f] Reference 59. [g] References 60 and 61. [h] Reference 62.

The S_1 states in both calculations are of 2 ^1A_g character with some mixing of the 1 ^1B_u state as a result of symmetry breaking by the deviation from planarity. The excitation energy of the S_2 state, which is approximately assigned as a 1 ^1B_u state in the C_{2h} point group, is 0.37 eV lower for the full TDDFT calculation than for the TDDFT/TDA calculation. Such a disagreement of the excitation energy of the 1 ^1B_u state has previously been systematically observed.[39] The transition dipole moment for $S_0 \rightarrow S_1$ is also significantly higher for the TDDFT result. This arises from a larger contribution of the 1 ^1B_u-like configuration, which is due to the smaller energy gap between the 2 ^1A_g-like and 1 ^1B_u-like configurations in TDDFT. In our previous study,[39] TDDFT systematically underestimated the excitation energy of 1 ^1B_u state by 0.4−0.5 eV for polyene oligomers when compared with the experimental values. For RG we believe the same systematic error is causing the smaller energy gap and thus unrealistically large mixing of 1 ^1B_u-like configuration with the S_1 (2 ^1A_g-like) state. In contrast, the TDDFT/TDA approach gave reasonable estimates of the energies for both states in polyene oligomers. Based on these results we believe that the transition properties of the first two excited states of RG would be more likely to be close to reality if calculated via TDDFT/TDA.

TABLE 3: Excited States of Molecule I, the Polyene Part of RG, from TDDFT/TDA and TDDFT Calculations Using SVWN/6-31++G, for the Two Different Geometries**

I, distorted[a] state	E^b	λ^c	f^d	μ^e	**I**, planar[f] state	E^b	λ^c	f^d	μ^e
TDDFT/TDA									
S_1	1.51	820.9	0.01	1.20	2^1A_g	1.91	649.7	0	0
S_2	2.12	585.7	1.53	13.8	1^1B_u	2.14	580.2	5.31	63.5
	2.23	555.4	5.96	26.5	2^1B_u	2.57	481.9	0.74	8.68
	2.41	513.8	3.73	20.2	3^1B_u	2.80	442.6	1.69	12.6
TDDFT									
S_1	1.50	824.5	0.11	4.36	1^1B_u	1.89	657.5	3.61	22.5
S_2	1.64	757.8	3.70	24.4	2^1A_g	1.91	649.7	0	0
	2.13	582.1	0.02	1.46	2^1B_u	2.54	488.8	0.24	5.00
	2.32	533.4	0.02	1.51	3^1B_u	2.73	454.1	0.32	5.51

[a] Crystal structure of RG with H atoms replacing the two end groups. [b] Excitation energies in electronvolts. [c] Excitation wavelengths in nanometers. [d] Oscillator strengths. [e] Transition dipole moments in Debye. [f] Optimized ground-state structure.

For consistency, the excited states of BChl *a* in B800 and B850 were calculated with the same level of TDDFT as used for RG. In Table 2 we summarize the results. The assignment of the Q_x and Q_y states is based on the magnitude and direction of the transition dipole moments. The direction of transition dipole moments for Q_x and Q_y states are known to point, approximately, along the Mg−N directions.[49] The calculated transition densities of these states are very similar to a previous CIS result.[50]

To gain insight into the mixing of S_2 with S_1, we also calculated the excited states of model molecule **I** resembling the conjugated core of RG. In Table 3 we summarize the results of our calculations on the two structures of **I**. The corresponding excitation energies of the first two states are about 0.3−0.4 eV lower in the distorted geometry, except for the case of the 2 ^1B_u (S_2) state in the TDDFT/TDA calculation. This result is related to the properties of excited-state gradients with respect to nuclear coordinates. While the problem of excited-state gradients for polyenes is an active area of research, for our current work there is not enough information for us to draw any significant conclusions from this result.

The Coulombic coupling between Q_y of BChls and the S_1 state of RG or its conjugated analogue (molecule **I**) are calculated using the transition density cube (TDC) method,[21] in which the transition density is represented by an array of charges on cubic grid points, and a direct summation of the Coulombic interaction between the two groups of charges is performed. The results are summarized in Table 4. To examine the consequence of symmetry breaking for RG, we have also included an analysis of coupling arising from A_g-like and B_u-like configurations. The S_1 wave function is composed of three major components in the Kohn−Sham orbital representation: HOMO → LUMO + 1, HOMO − 1 → LUMO and HOMO → LUMO. The amplitudes of these three configurations in RG are −0.6923, +0.7174, and −0.0672, respectively. The first two components form a configuration that resembles A_g symmetry, consisting of more than 99% of the population. The last

TABLE 4: Coulombic Coupling (cm^{-1}) of S_1 Transitions of $RG1_B$ and Molecule I with Its Neighboring BChl Q_yTransitions[a]

state	$\alpha B850_B$[b]	$\beta B850_B$	$\alpha B850_C$	$\beta B850_C$	$B800_A$	$B800_B$
Rhodopin Glucoside (Full Columbic Coupling)[c]						
S_1	−4.8	9.1	32.2	−18.0	31.4	−9.8
A_g-like	6.8	5.0	16.6	0.2	−16.6	5.5
B_u-like	−10.9	8.5	27.3	−22.7	43.6	−13.0
Rhodopin Glucoside (Dipole−Dipole Coupling)						
S_1	−16.7	−10.7	13.3	−9.8	48.7	−23.0
A_g-like	6.1	−1.0	−3.4	4.2	−26.0	0.2
B_u-like	−23.4	−11.0	18.2	−15.4	73.1	−29.9
Rhodopin Glucoside (Multipole Approximation)[d]						
S_1	−4.3	−0.41	19.8	−10.9	45.7	43.0
A_g-like	10.4	−2.9	−16.9	9.3	−43.8	36.1
B_u-like	−15.3	3.3	35.1	−21.3	81.9	2.6
Molecule I (Distorted)[c]						
S_1	−3.2	6.8	19.2	−13.7	27.6	−8.6
A_g-like	5.9	5.1	7.7	−0.1	−25.9	9.2
B_u-like	−7.6	4.6	18.1	−17.8	44.3	−13.1
Molecule I (Planar)[c]						
S_1 (2^1A_g)	2.1	14.5	25.0	−9.6	15.8	−8.2

[a] Coupling arising from two major components of the S_1 state are listed. [b] The labeling scheme of BChls follows that in ref 21, which is indicated in Figure 3. [c] Full Coulombic coupling calculated using TDC. [d] The multipole coupling is a sum of dipole−dipole, quadrupole-dipole, octapole-dipole, and quadrupole-quadrupole couplings.

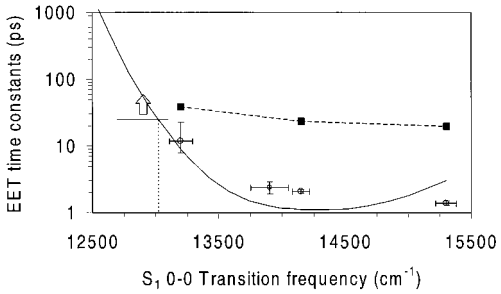

Figure 4. EET rate vs the Car S_1 0−0 transition energy. Our ensemble-averaged result is plotted as the solid line, assuming that the couplings with BChls, the excitation spectra of the S_1 state of different carotenoids, and the BChls Q_y excitonic state distribution are all the same. Filled squares connected by a dashed line are a result of an earlier estimate reported in ref 18. Open circles with error bars are experimental results reported in refs 16 and 18. The horizontal bar with an arrow at the left is to indicate an experimental result for LH2 in *Rps. acidophila*, where a lower bound of 25 ps is reported for the EET time constant.[16] The spectral position of S_1 of RG is not known. From our result we infer an upper bound of 13 000 cm^{-1} for the 0−0 transition frequency.

component is a small mixing from the $1\ ^1B_u$ state due to symmetry breaking. Such a configuration has a large transition dipole moment. Couplings from the A_g-like and the B_u-like configurations to nearby BChl's in the LH2 structure are also included in Table 4. The distorted molecule **I** behaves in a similar manner. The coefficients of the three configurations mentioned above, in the same order, are −0.6961, +0.7145, and −0.0556. The couplings from the A_g-like and the B_u-like components are calculated similarly, and the results are listed in Table 4. For the planar molecule **I** it is optimized in its ground state, which is a planar structure with C_{2h} symmetry. Therefore the S_1 state is rigorously assigned as the $2\ ^1A_g$ state. There is no symmetry breaking. In this case, there is no need to separate the configuration of the $2\ ^1A_g$ state into different components.

In Figure 4 we plot the dependence of the ensemble-averaged EET rate as a function of the S_1 0−0 transition frequency, keeping the coupling between Car(S_1) and Bchl(Q_y) fixed at the TDDFT/TDA values reported in Table 4. For comparison, several other results from experiments or theoretical calculations[18,16] are also included in this plot.

IV. Discussion

A. Car(S_1)−BChl(Q_y) Coupling. From the results listed in Table 4 we can see that, for rhodopin glucoside in the crystal structure, the B_u-like configuration plays a larger role than the A_g-like configuration in the coupling with nearby BChls, although the A_g-like couplings are not negligible. The signs of Coulombic couplings of the S_1 state follow that of the B_u-like configuration, indicating that the Coulombic coupling of the B_u-like component is dominant. This result looks even more remarkable when one realizes that the B_u-like configuration considered here has an amplitude of only −0.0672, or 0.45% in the population. To investigate this effect further, we note that RG has different groups on the two ends, and more importantly, in the crystal structure RG is distorted from a planar geometry (Scheme 1 and Figure 3).

Deleting the two functional groups at both ends of the conjugated part of RG leads to the distorted structure of molecule **I**. In Table 4 we see a similar trend comparing the influence from the A_g-like component to that of the B_u-like one. Generally, compared to the coupling of the entire RG molecule, the overall coupling magnitudes are reduced by about 10% for the B800 BChls and by about one-third for the B850 BChls. This is accounted for by the close proximity of the B850 BChls to the alkenyl group (4-methyl 3-pentenyl group) that has been deleted in the model molecule. Coupling with $\alpha B850_C$ is reduced the most among the four B850 BChls studied, since $\alpha B850_C$ is the BChl that has the closest contact with the deleted alkenyl group.

In the couplings with the two B800 BChls and $\alpha B850_B$, the A_g-like configuration is opposite in sign to the overall Coulombic coupling. The sign of Coulombic coupling reflects the phase of transition density, which is a result of the combined phases of the wave functions. Since the B_u-like component, which dominates the Coulombic coupling of the S_1 state is dipolar in nature, while the A_g-like component has a high-order transition moment (the transition density of this part closely resembles that plotted in Figure 2), the electric potential created by the two components have different signs (phases) in certain regions of space, causing different signs for the Coulombic interaction with the transition densities of BChls at some of the sites.

For the planar polyene molecule **I** there is no such mixing of a B_u component. The results for the Coulombic coupling to the neighboring BChls show that the coupling strengths are in general slightly smaller than that of RG. However, the substantial values of these Coulombic couplings from a molecule without a transition dipole moment clearly show that a transition moment is *not* a requirement for significant Coulombic coupling. This result is contrary to the common practice of assuming that orbital overlap (exchange) coupling must dominate when the transition is weak or entirely forbidden.

Comparing the results from planar and distorted model molecule **I**, the displacements of atomic positions cause some fluctuation in the coupling strengths. For example, the *increase* of coupling strength in $\beta B850_B$ and $\alpha B850_C$ as the molecule becomes more symmetric is likely due to the fact that the terminal carbon atoms are actually moved closer to the two BChls when the model molecule **I** becomes planar. Therefore it is not very meaningful to discuss in detail the changes of the coupling in these cases.

One curious observation, however, arises from the signs of the couplings from the A_g-like component of the distorted molecule **I** and the 2 ^1A_g state of the planar molecule. In this case they are both nondipolar in nature so the above discussion of different signs (phases) of electric potential arising from different multipolar character in transition density does not apply. The transition densities of the A_g-like component of the distorted molecule and the 2 ^1A_g state of the planar molecule **I** are very similar to that shown in Figure 2, representing a linear array of alternating sign charge clouds, except that the location and the arrangement of the charge clouds are different since they follow the locations of the conjugated double bonds. Such charge distribution is like a high-order multipole, creating a roughly cylindrically symmetric potential with alternating signs across the polar angle. In other words, the electric potential created by such charge distribution has many curved "nodal planes" where the electric potential changes its sign. Such nodal planes would have been cone-shaped if the source were an ideal point multipole. A distortion of the molecule leads to displacement and distortion of such nodal planes and as a result, the Coulombic interaction may change sign. We believe the origin of the change in sign of the B800 coupling is the shifted nodal plane(s) of potential at the region, which results from bending the polyene molecule.

There is a particularly small coupling strength, 0.2 cm^{-1}, between the A_g-like configuration of the carotenoid and the BChl at the $\beta B850_C$ position. The corresponding result for the model molecule **I** in the crystal structure configuration is essentially the same. We believe that this is a mathematical result for a Coulombic coupling arising from two transition densities that have a large number of nodal planes. A shift of molecular position by 2 Å would change the coupling to -1.2 cm^{-1}. In a realistic situation, this coupling is not likely to be so small at such a moderate distance from the acceptor since a small variation in the atomic position (e.g., via vibration) and in the description of wave function would significantly increase such small couplings.

From the results listed in Table 4 we can conclude that (1) the B_u-like configuration couples strongly to its neighbors. Therefore even with a very small ($<0.5\%$ in population) mixing it still contributes significantly to the Coulombic coupling of RG with BChl. (2) The strength of the A_g component may vary depending on the nature of the molecule. Such a variation produces different couplings for molecule **I** and the A_g-like component of RG. (3) A transition dipole moment is *not* a necessary condition for a transition to couple strongly with (allowed) transitions of other molecules.

At this point it seems appropriate to discuss the accuracy of our calculations. Uncertainties arise from errors in the positions of the heavy atoms obtained from the experimental structure, as well as errors intrinsic to the TDDFT approach. However for RG an incorrect coefficient of the B_u-like configuration in the S_1 state leads to a large transition dipole moment, which can be compared to experimental results. Our results for RG with the full form of TDDFT fall into this category: they yield a large transition dipole moment (6.6 D, oscillator strength of 0.25) for S_1 that should have been easily observed in standard absorption/emission spectra. As noted earlier, the large oscillator strength is due to a large mixing coefficient of a B_u-like component, which arises from an underestimation of the energy of the S_2 (1 ^1B_u) state. As a result the S_2 state is unrealistically close to the S_1 state, leading to a larger perturbative mixing of S_2 (1 ^1B_u) character in the S_1 (2 ^1A_g) transition. A simple test showed that the Coulombic coupling is indeed several times larger than the values obtained from TDDFT/TDA calculations.

On the other hand, it is less straightforward to determine the accuracy of calculation for the A_g-like components or for the 2 ^1A_g state of totally symmetric polyenes. However we find that, for a carotenoid in the LH2 structure, its coupling to nearby BChls is not strongly sensitive to a change in the strength of the A_g transition densities. The coupling with the BChls is slightly larger for the planar molecule **I** than for the A_g-like component of RG. The detailed geometry of the molecule has certainly an effect on the form of the transition density, as discussed above. As can be seen from Table 4, such variation is appreciable but the total coupling is smaller in magnitude than that arising from the B_u-like component.

The Car(S_1)−BChl(Q_y) coupling strengths we obtained are larger than the couplings suggested earlier by Zhang et al.,[18] in which the weak S_1 emission of carotenoids *in solution*, possibly arising from vibronic coupling, is used to estimate the amount of S_1-Q_y coupling. The coupling strengths for all the three carotenoids found in the three LH2 complexes studied were estimated to be 4−6% of the corresponding S_2-Q_y couplings, about a factor of 3 smaller than the 15% estimated by the fitting procedure described in ref 16, to which our calculated results are very close. There is also a major difference in estimating the energy conservation (i.e., spectral overlap) factor, which will be discussed in the following section.

B. Excitation Energy Transfer Rate and the Position of Car S_1 State. To determine an EET rate from the individual couplings, we need to determine the position of the spectral density of the carotenoid S_1 state, i.e., the 0−0 transition frequency. In Figure 4 we show the dependence of the EET rate on the S_1 0−0 transition frequency, keeping the coupling between pigments and the spectral profiles fixed. The figure shows that the trends in the experimental results from different LH2 complexes are reproduced by our calculations.

The 0−0 transition frequency has been determined to be around 13 900 or 14 150 cm^{-1} for spheroidene in LH2 of *Rb. sphaeroides* 2.4.1.[15,18] From Figure 4 we can see that the overall EET rate is quite insensitive to the 0−0 transition in this frequency range, based on the assumption that the structure and couplings in LH2 of *Rb. sphaeroides* are the same as those of *Rps. acidophila*. In this case the overall Car(S_1) → BChl(Q_y) EET rate is determined to be 1.2 ps, which compares well to the experimental results of 2.4[16] and 2.1 ps.[18]

For *Rps. acidophila* the 0−0 transition of S_1 of RG is estimated to be about 13 000 cm^{-1}, according to studies on other carotenoids with the same number (11) of conjugated double bonds.[18] In this range, the energy transfer rate depends strongly on the 0−0 transition frequency. (See Figure 4; also see the inset of Figure 5 in ref 16.) The agreement of theoretical calculation with experimental results for *Rps. acidophila* can only be roughly assessed. From our recent experimental work,[16] the EET time constant was determined to be greater than 25 ps, leading to an estimate of the S_1 0−0 transition for RG in LH2 as being about 13 000 cm^{-1} or lower.

For the LH2 complex from *Rs. molischianum*, we have obtained an EET time constant of 9.0 ps by shifting the S_1 0−0 transition frequency to 13 200 cm^{-1} (as suggested in ref 18), which is very close to the experimental results of 12.3 ps.

For the LH2 from *Rb. sphaeroides* G1C, which has neurosporene as its carotenoid, we estimate the EET time constant to be 3.0 ps, which compares well with the experimental value of 1.4 ps.[18] In this case the S_1 0−0 transition frequency is set to 15 300 cm^{-1}, as suggested in ref 18.

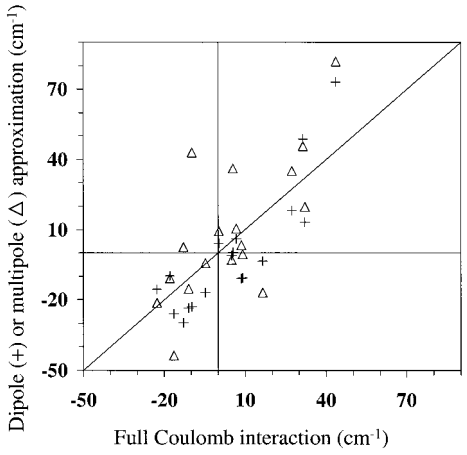

Figure 5. Comparison of full Coulombic coupling and dipole or multipole approximation. "+" denotes the dipole−dipole approximation, and the triangles denote the multipole approximation for a summation of dipole−dipole, dipole−quadrupole, dipole-octapole, and quadrupole-quadrupole interactions.

The B800−B850 LH2 complexes from *Rps. acidophila*, *Rs. molischianum*, and *Rb. sphaeroides* are known to have similar chemical and spectroscopic properties.[51−53] The crystal structure of LH2 in *Rs. molischianum* is not exactly the same as that of *Rps. acidophila*.[9] In addition to the different arrangements of BChls in the B800 and B850 rings, the LH2 complexes from these species contain carotenoids differing in the functional groups at both ends and in the number of conjugated double bonds. Clearly these differences will lead to variation in the coupling between Cars and BChls. The success in describing the EET rate in LH2 of *Rb. sphaeroides* and *Rs. molischianum* in the present work can be interpreted as implying that the Coulombic coupling between Car(S_1) and BChl(Q_y) are roughly similar in their magnitudes. Therefore the following conditions are also implied: (1) mixing of B_u-like character in the S_1 state of spheroidene, lycopene, and neurosporene do not vary much from that in RG in these LH2 complexes. The extent of mixing of the B_u-like character is dependent on the energy gap between the S_1 and S_2 states and the extent of geometry distortion in the protein matrix. At this point the detailed geometry for the LH2 complexes from *Rb. sphaeroides* is unknown, while for the LH2 from *Rs. molischianum* the crystal structure is available and can be further investigated. (2) Coulombic coupling is mostly determined by the main features of the transition density. The detail of the excited-state wave function is not as important as the main features of the wave function in determining the coupling strength. The success of a simple ab initio calculation performed with CIS and a small basis set for the S_2 states of the carotenoid supports this observation.[21] We expect that the transition density of spheroidene, lycopene, and neurosporene should be roughly similar to RG locally despite the differences in their chemical structures. The number of conjugated double bonds is not the same for each carotenoid. Similarly, in ref 20, model molecules of 10 conjugate double bonds were used in the calculation to replace lycopene, which has 11 conjugated double bonds, and the Coulombic couplings of Car(S_2) and BChl (both Q_x and Q_y) are reasonably described.

The interaction between each chromophore pair may not be exactly the same in all the four different LH2 complexes that we have compared our calculated EET rates with, but overall the coupling may be quite similar to that of LH2 from *Rps. acidophila*, which the present study is based on. We are currently working on a similar calculation of LH2 in *Rs. molischianum*. These results should enable us to address the role of structual variations in LH2 complexes.

C. Multipole Approximation. Our conclusion that the dipole-allowed B_u-like component in the S_0 to S_1 transition makes the major contribution to the Car(S_1)−BChl(Q_y) coupling raises the question of whether such coupling can be simplified to a Förster dipole coupling. In the literature, a quadrupole−dipole coupling scheme has often been proposed and was discussed for this particular system as an alternative to the traditional dipole coupling scheme.[17]

In Table 4 we list the coupling strengths from dipole and multipole approximations (in parentheses) for the Car−BChl pairs. The multipole coupling is a summation of the lowest order terms in multipole expansion which include dipole−dipole, dipole−quadrupole, dipole−octapole, and quadrupole−quadrupole coupling. Comparing these values with the transition density cube results, we conclude that dipole−dipole coupling is not a good approximation in this case, even though the configuration that contributes the most to coupling (the B_u-like component) has a large transition dipole moment. In addition, the multipole approximation does *not* offer any improvement of the estimates (Figure 5).

As pointed out before,[21] the multipole approximation breaks down for most intermolecular distances studied in the present work. The multipole expansion uses a set of spherical harmonic functions to reproduce the electric potential of a charge distribution. It is performed to reproduce the electric potential *outside* a sphere of radius *R*, while the source charges are confined *within* the sphere.[54] In other words, to determine the interaction between two groups of charges by multipole expansion, the sphere enclosing each group of charges must not overlap. The 11 conjugated double bonds of RG, which are roughly 26 Å in length, makes *R* at least 13 Å. The neighboring BChls have atoms much closer to the center of RG than this (Figure 2). Therefore, the multipole expansion is not valid for estimating the Coulombic interaction between RG and its neighboring BChls since the fundamental assumption in performing multipole expansion is violated in this case. Indeed, the multipole results included in Table 4 and Figure 5 do not offer any improvement in the quality of estimation over the dipole approximation. This observation demonstrates that the discrepancy between full Coulombic coupling and the dipole approximation in this case *is not* due to a multipole interaction term.

D. TDDFT on Bacteriochlorophylls: Additional States Found in the Q_y Region. In Table 2 we listed the first four excited states obtained for each BChl. We have assigned Q_x and Q_y states according to the direction and magnitude of transition dipole moments, as listed in Table 2.[49] Such an assignment is supported by the high similarity of the transition densities of these states and the ones from a previous CIS calculation.[50] In additional to the Q_y state, there is at least one additional state lower in energy than the Q_x state.

A previous calculation with TDDFT showed that the phytyl group has very little effect on excitation energies and oscillator strengths of the lower excited states obtained for the chlorophyll (Chl) *a* molecule near the region of the Q-band.[37] Such calculations also generate more than two electronic states within the region of the Q_x and Q_y bands.[36] TDDFT is likely the first ab initio study on the excited states of chlorophylls or other similar molecules that does not involve a selection of active electrons and active space in configuration interaction. However, it heavily relies on a few approximations that exist in the currently available exchange-correlation functionals. More work

is clearly needed to address the validity of new states obtained by TDDFT calculations in the low-frequency region.

E. Dark State between S_1 and S_2? Recent experimental studies on carotenoids have suggested the existence of a $^1B_u^{(-)}$ state between 2 $^1A_g^{(-)}$ and 1 $^1B_u^{(+)}$ states.[55] The alternacy symmetry and point group symmetry assignment indicates this additional state as one- and two-photon forbidden. However, in our calculation, the lowest few excited states with B_u symmetry always have a strong oscillator strength for their transition from the ground state.

The alternacy symmetry is exact within the PPP semiempirical Hamiltonian, where the coupling of π orbitals are limited to the nearest neighbors. For a full SCF calculation with either Hatree-Fock theory or density functional theory, the molecular (Kohn−Sham) orbital energies do not form pairs of $\epsilon \pm \epsilon_n$ as described in the literature.[20,56,57] Therefore the rules derived from the alternacy symmetry are only approximately valid in our results, even for the strictly symmetric polyenes. We would then expect a mixing of strongly one-photon allowed 1 $^1B_u^+$ character in all the B_u^- states, adding a transition dipole moment to all the B_u^- states.

On the other hand, it is possible that such a three-photon-allowed state exists at higher energies in the TDDFT calculation. In the present study the results listed in Table 1 do not provide enough information to draw such a conclusion. It is possible that the properties of the two higher excited states in our calculations will change when the number of excited states calculated is increased.

V. Conclusion

The EET coupling strengths between the S_1 state of carotenoids and the Q_y state of nearby BChls in the LH2 complex of *Rps. acidophila* are obtained from TDDFT calculations. The overall EET rates calculated on the basis of the Coulombic couplings obtained in the present study and the excitonic model employed in an earlier work[47] are in excellent agreement with experimental results from different LH2 complexes. The mixing of a B_u-like component due to symmetry breaking is shown to play an important role in determining the EET coupling strengths of Car S_1 with other pigments. Therefore, it is essential to describe the amount of mixing of the B_u-like component in the Car S_1 state correctly in an electronic structure calculation. However, it is also clear that reasonably strong Coulombic coupling can arise simply from the spatial proximity inherent in the asymmetric arrangement of donors and acceptors in LH2, even when the transition moment is rigorously zero. The dipole approximation for the Coulombic coupling is shown to be invalid in the LH2 complex. The multipole approximation, with a summation including up to the fourth-order expansion term, shows no sign of convergence. Standard approaches for calculating EET couplings with dipole or multipole approximations are not appropriate in the case of LH2.

Acknowledgment. C.P.H. gratefully acknowledges a fellowship from the Miller Institute for Basic Research in Science. This work was supported by the Director, Office of Science, Office of Basic Energy Sciences, Chemical Sciences Division, of the U.S. Department of Energy under Contract No. DE-AC03-76SF0098.

References and Notes

(1) For example: Van Amerongen, H.; Valkunas, L.; Van Grondelle, R. *Photosynthetic Excitons*; World Scientific Publishing Co.: Singapore, 2000.

(2) Govindjee. In *The photochemistry of Cartenoids*; Frank, H. A., Young, A. J., Britton, G., Cogdell, R. J., Eds.; Kluwer Academic Publishers: Dordrecht, The Netherlands, 1999; pp 1−19.

(3) Dutton, H. J.; Manning, W. M.; Duggar, B. M. *J. Phys. Chem.* **1943**, *47*, 308.

(4) Duysens, L. N. M. *Nature* **1951**, *168*, 548.

(5) Frank, H. A.; Cogdell, R. J. *Photochem. Photobiol.* **1996**, *63*, 257.

(6) Koyama, Y.; Kuki, M.; Andersson, P. O.; Gillbro, T. *Photochem. Photobiol.* **1996**, *63*, 243.

(7) Krinsky, N. I. The protective function of carotenoid pigments. In *Photophysiology*; Giese, A. C., Ed.; Academic Press: New York 1968; Vol. 3, pp 123−195. Krinsky, N. I. Function. In *Carotenoids*; Isler, O., Ed.; Birkhauser Verlag: Basel and Stuttgart, 1971; pp 670−716.

(8) McDermott, G.; Prince, S. M.; Freer, A. A.; Hawthornthwaite-Lawless, A. M.; Papiz, M. Z.; Cogdell, R. J.; Isaacs, N. W. *Nature* **1995**, *374*, 517.

(9) Koepke, J.; Hu, X.; Muenke, C.; Schulten, K.; Michel, H. *Structure* **1996**, *4* 581.

(10) Krueger, B. P.; Scholes, G. D.; Jimemez, R.; Fleming, G. R. *J. Phys. Chem. B* **1998**, *102*, 2284.

(11) Andersson, P. A.; Cogdell, R. J.; Gillbro, T. *Chem. Phys.* **1996**, *210*, 195.

(12) Macpherson, A. N.; Arellano, J. B.; Fraser, N. J.; Cogdell, R. J.; Gillbro, T. In *Photosynthesis: Mechanisms and Effects*; Kluwer Academic Publishers: Dordrecht, Netherlands. 1998; Vol I, pp 9−14.

(13) Desamero, R. Z. B.; Chynwat, V.; Van der Hoef, I.; Jansen, F. J.; Lutenburgm, J.; Gosztola, D.; Wasielewski, M. R.; Cua, A.; Bocian, D. F.; Frank, H. A. *J. Phys. Chem. B* **1998**, *102*, 8151.

(14) Shreve, A. P.; Trautman, J. K.; Frank, H. A.; Owens T. G.; Albrecht, A. C. *Biochim. Biophys. Acta* **1991**, *1058*, 280.

(15) Krueger, B. P.; Yom, J.; Walla, P. J.; Fleming, G. R. *Chem. Phys. Lett.* **1999**, *310*, 57.

(16) Walla, P. J.; Linden, P. A.; Hsu, C.-P.; Scholes, G. D.; Fleming, G. R. *Proc. Natl. Acad. Sci. U.S.A.* **2000**, *97*, 10808.

(17) Nagae, H.; Kakitani, T.; Katoh T.; Mimuro, M. *J. Chem. Phys.* **1993**, *98*, 8012.

(18) Zhang, J.-P.; Fujii, R.; Qian, P.; Inaba, T.; Mizoguchi, T.; Joyama, Y.; Onaka, K.; Watanabe Y.; Nagae, H. *J. Phys. Chem. B* **2000**, *104*, 3683.

(19) Alden, R. G.; Johnson, E.; Nagarajan, V.; Parson, W. W.; Law, C. J.; Cogdell, R. G. *J. Phys. Chem. B* **1997**, *101*, 4667.

(20) Damjanović, A.; Ritz, T.; Shulten, K. *Phys. Rev. E* **1999**, *59*, 3293.

(21) Krueger, B. P.; Scholes, G. D.; Fleming; G. R. *J. Phys. Chem.* **1998**, *102*, 5378.

(22) Scholes, G. D.; Gould, I. R.; Cogdell, R. G.; Fleming, G. R. *J. Phys. Chem. B* **1999**, *103*, 2543.

(23) Förster, Th. *Ann. Phys.* **1958**, *2*, 55.

(24) Dexter, D. L. *J. Chem. Phys.* **1953**, *21*, 836.

(25) Runge, E.; Gross, E. K. U. *Phys. Rev. Lett.* **1984**, *52*, 997.

(26) Gross, E. K. U.; Kohn, W. *Adv. Quantum Chem.* **1990**, *21*, 255.

(27) Casida, M. E. In *Recent Advances in Density Functional Methods*; Chong, D. P., Ed.; World Scientific Publishing Co. Ltd.: Singapore, 1995; pp 155−192.

(28) Gross, E. K. U.; Ullrich, C. A.; Gossmann, U. J. In *Density Functional Theory*; Gross, E. K. U., Driezler, R. M., Eds.; Plenum Press: New York, 1995; pp 149−171.

(29) Petersilka, M.; Gossmann, U. J.; Gross, E. K. U. *Phys. Rev. Lett.* **1996**, *76*, 1212.

(30) Jamorski, C.; Casida, M. E.; Salahub, D. R. *J. Chem. Phys.* **1996**, *104*, 5134.

(31) Bauernschmitt R.; Ahlrichs, R. *Chem. Phys. Lett.* **1996**, *256*, 454.

(32) Bauernschmitt R.; Haser, M.; Treutler, O.; Ahlrichs, R. *Chem. Phys. Lett.* **1997**, *264*, 573.

(33) Stratmann, R. E.; Scuseria, G. E.; Frisch, M. J. *J. Chem. Phys.* **1998**, *109*, 8218.

(34) Hirata, S.; Lee, T. J.; Head-Gordon, M. *J. Chem. Phys.* **1999**, *111*, 8904.

(35) Hirata, S.; Head-Gordon, M. *Chem. Phys. Lett.* **1999**, *302*, 375.

(36) Sundholm, D. *Chem. Phys. Lett.* **1999**, *302*, 480.

(37) Sundholm, D. *Chem. Phys. Lett.* **2000**, *317*, 545.

(38) Hirata, S.; Head-Gordon, M. *Chem. Phys. Lett.* **1999**, *314*, 291.

(39) Hsu, C.-P.; Hirata, S.; Head-Gordon M. *J. Phys. Chem. A* **2001**, *105*, 451.

(40) Casida, M. E.; Jamorski, C.; Casida K. C.; and Salahub, D. R. *J. Chem. Phys.* **1998**, *108*, 4439.

(41) Hsu, C.-P.; Fleming, G. R.; Head-Gordon, M.; Head-Gordon, T. *J. Chem. Phys.* **2001**, *114*, 3065.

(42) Kong, J.; White, C. A.; Krylov, A. I.; Sherrill, C. D.; Adamson, R. D.; Furlani, T. R.; Lee, M. S.; Lee, A. M.; Gwaltney, S. R.; Adams, T. R.; Ochsenfeld, C.; Gilbert, A. T. B.; Kedziora, G. S.; Rassolov, V. A.; Maurice, D. R.; Nair, N.; Shao, Y.; Besley, N. A.; Maslen, P. E.; Dombroski, J. P.; Daschel, H.; Zhang, W.; Korambath, P. P.; Baker, J.; Byrd, E. F. C.; Van Voorhis, T.; Oumi, M.; Hirata, S.; Hsu, C.-P.; Ishikawa, N.; Florian, J.;

Warshel, A.; Johnson, B. G.; Gill, P. M. W.; Head-Gordon M.; Pople, J. A. *J. Comput. Chem.* **2000**, *21*, 1532.

(43) Becke, A. D. *J. Chem. Phys.* **1993**, *98*, 5648.

(44) Slater, J. C. *The Self-Consistent Field for Molecules and Solids*; Quantum Theory for molecules and Solids; McGraw-Hill: New York, 1974; Vol. 4.

(45) Vosko, S. H.; Wilk, L.; Nusair, M. *Can. J. Phys.* **1980**, *68*, 1200.

(46) Damjanović, A.; Ritz, T.; Shulten, K. *Biophys. J.* **2000**, *79*, 1695.

(47) Scholes, G. R.; Fleming, G. R. *J. Phys. Chem. B* **2000**, *104*, 1854.

(48) He, Z.; Sundström, V.; Pullerits, T. *Chem. Phys. Lett.* **2001**, *334*, 159.

(49) For example: Van Amerongen, H.; Valkunas, L.; Van Grondelle, R. *Photosynthetic Excitons*; World Scientific Publishing Co.: Singapore, 2000; pp 76−77.

(50) Krueger, B. P. The Role of Carotenoids in Bacterial Light hargesting. Ph.D. Thesis, University of Chicago, Chicago 1999.

(51) Beekman, L. M. P.; Frese, R. N.; Fowler, G. J. S.; Picorel, R.; Cogdell, R. J.; van Stokkum, I. H. M.; Hunter, C. N.; van Grondelle, R. *J. Phys. Chem. B* **1997**, *101*, 7293.

(52) Gottfried, D. S.; Stocker, J. W.; Boxer, S. G. *Biochim. Biophys. Acta* **1991**, *1059*, 63.

(53) Koolhaas, M. H. C.; Frese, R. N.; Fowler, G. J. S.; Bibby, T. S.; Georgakopoulou, S.; van der Zwan, G.; Hunter C. N.; van Grondelle, R. *Biochemistry* **1998**, *37*, 4693.

(54) Jackson, J. D. *Classical Electrodynamics*, 2nd ed.; John Wiley & Sons Inc.: Singapore, 1975; p 137.

(55) Sashima, T.; Nagae, H.; Kuki, M.; Koyama, Y. *Chem. Phys. Lett.* **1999**, *299*, 187.

(56) Pariser, R. *J. Chem. Phys.* **1956**, *24*, 250.

(57) Koutecky, J. *J. Chem. Phys.* **1966**, *44*, 3702.

(58) Andersson, P. O.; Gillbro, T.; Ferguson, L.; Cogdell, R. J. *Photochem. Photobiol.* **1991**, *54*, 353.

(59) Budil, D. E.; Gast, P.; Chang, C. H.; Schiffer M.; Norris, J. *Annu. Rev. Phys. Chem.* **1987**, *38*, 561.

(60) Shatz, G. H.; Brock, H.; Holzwarth, A. R. *Proc. Natl. Acad. Sci. U.S.A.* **1987**, *84*, 8414.

(61) Causgrove, T. P.; Yang, S.; Struve, W. S. *J. Phys. Chem.* **1988**, *92*, 6121.

(62) Sauer, K.; Smith, J. R. L.; Schultz, A. J. *J. Am. Chem. Soc.* **1966**, *88*, 2681 1966.